Distal end force sensing with optical fiber Bragg gratings for tendon-sheath mechanisms in flexible endoscopic robots

Lai, Wenjie; Cao, Lin; Xu, Zhilin; Phan, Phuoc Thien; Shum, Ping; Phee, Soo Jay

2018

Lai, W., Cao, L., Xu, Z., Phan, P. T., Shum, P., & Phee, S. J. (2018). Distal end force sensing with optical fiber Bragg gratings for tendon-sheath mechanisms in flexible endoscopic robots. Proceedings of 2018 IEEE International Conference on Robotics and Automation (ICRA), 5349-5355. doi:10.1109/ICRA.2018.8461090

https://hdl.handle.net/10356/137867

https://doi.org/10.1109/ICRA.2018.8461090

Distal End Force Sensing with Optical Fiber Bragg Gratings for Tendon-Sheath Mechanisms in Flexible Endoscopic Robots

Wenjie Lai[1], Lin Cao[1*], Zhilin Xu[2*], Phuoc Thien Phan[1], Ping Shum[2], Soo Jay Phee[1]

***Abstract*— Accurate haptic feedback is a critical challenge for surgical robots, especially for flexible endoscopic surgical robots whose transmission systems are Tendon-Sheath Mechanisms (TSMs) with highly nonlinear friction profiles and force hysteresis. For distal end haptic sensing of TSMs, this paper, for the first time, proposes to measure the compression force on the sheath at the distal end so that the tension force on the tendon, which equals the compression force on the sheath, can be obtained. A new force sensor, i.e., a nitinol tube attached with an optical Fiber Bragg Grating (FBG) fiber, is proposed to measure the compression force on the sheath. This sensor, with similar diameter and configuration (hollow) as the sheath, can be compactly integrated with TSMs and surgical end-effectors. In this paper, mechanics analysis and verification tests are presented to reveal the relationship between the tension force on the tendon and the compression force on the sheath. The proposed force sensor was calibrated in tests with a sensitivity of 24.28 pm/N and integrated with a tendon-sheath driven grasper to demonstrate the effectiveness of the proposed approach and sensor. The proposed approach and sensor can also be applied for a variety of TSMs-driven systems, such as robotic fingers/hands, wearable devices, and rehabilitation devices.**

***Index Terms*— Haptic Sensing, Fiber Bragg Gratings, Flexible Surgical Endoscopic Robot, Tendon-Sheath Mechanisms.**

I. INTRODUCTION

Minimally Invasive Surgery (MIS) has become an effective treatment since its introduction by John Wickham in 1986 [1]. By minimizing the incision, MIS brings dramatic benefits to patients, such as reduced hospital stays, less pain, lower postoperative infection rates and better cosmetic results [2]. In accordance with MIS, utilizing natural orifices (i.e. mouth, vagina, anus, etc.) as an entry point, Natural Orifice Transluminal Endoscopic Surgery (NOTES) leaves no visible scars after surgery [3]. Both MIS and NOTES have attracted tremendous interests in developing robotic systems for the associated surgical procedures. Robotic surgical systems are beneficial to surgeons in terms of improved precision, better vision, improved dexterity, and less fatigue and are also beneficial to patents in terms of further reduced incisions, faster recovery, and better cosmetic. Till now, significant technological advances have been achieved, and robot-assisted MIS systems are now becoming increasingly popular in clinic [4]. However, one common problem with existing robotic surgical systems is the absence of accurate haptic feedback. Studies have shown that adding accurate haptic feedback to the hands of the surgeon not only reduces the cases of excessive forces to avoid damaging the tissue and/or the instrument but also significantly shorten intraoperative time [5-7]. Nevertheless, this is not possible without accurate real-time force information at the distal end of the robot.

In the literature, there are generally two ways to obtain the force information at the distal ends of surgical robots. The first one is to sense the force at the proximal side and to predict the force at the distal side by modelling the transmission mechanisms of the robot; the second way is to directly mount force sensors to the distal side of the instrument.

In NOTES robotic systems, Tendon-Sheath Mechanisms (TSMs) [3, 8, 9] are widely adopted for force and motion transmission because of their compact sizes, flexibility in shape configurations, and reliability for high payloads. However, modeling the force transmission of shape-changing TSMs are challenging because of the backlash, nonlinear friction, and hysteresis with TSMs [10, 11]. Kaneko et al [12] analyzed the tension transmission in TSMs using the Coulomb friction model. Additionally, Chen et al. [13] studied the position and force transmission models of single-tendon-sheath actuation system. Wang et al. [14] compared tissue modelling methods inclusive of Maxwell model, Voigt model and Kelvin model and developed a force transmission model to predict the tissue force reaction of a flexible surgical endoscopic robot. Furthermore, Do et al [10] proposed a dynamic friction model to fit and predict nonlinear hysteresis behaviors of TSMs. Nevertheless, these approaches are generally dependent on external loads and the sheath configurations which keep changing during the surgery and thus may not provide accurate force prediction during the surgery.

Directly mounting force sensors to the distal end of a surgical robot is an alternate promising solution for haptic feedback. In the literature, eight sensing principles based on displacement [15], current [16], pressure [17], resistance [18], capacitance [19], piezoelectricity [20], vibration [21] and optical properties [22] have been explored for MIS. All these sensors are installed on the end-effectors of the instruments which have direct contact with surgical objects. Unfortunately, most of these force sensors with electrical cable connections encounter problems such as large sizes, complexities due to wires and accessories, and temporal hysteresis. Meanwhile, electrical sensors are susceptible to electromagnetic interference so that the accuracy can be a challenge and they are not suitable for MRI environment. Among these sensors, MEMS-based (Microelectro-mechanical systems) are also promising because of their small sizes, good spatial resolution, and

[1]W. J. Lai, L. Cao, P. T. Phan, and S. J. Phee are with Robotics Research Center, School of Mechanical and Aerospace Engineering, Nanyang Technological University, Singapore.

[2]Z. L. Xu and P. Shum are with Center for Optical Fiber Technology, School of Electrical and Electronic Engineering, Nanyang Technological University, Singapore.

[*]Correspondence to lin.cao@ntu.edu.sg, zlxu@ntu.edu.sg

multi-axis DOFs detections [23]. Nevertheless, such sensing approach still poses problems like fragile sensing elements, rigid substrates, transmission loss, noises, signal processing, MRI-incompatibility, and space requirements for accessories [24].

Compared to above mentioned sensors, Fiber Bragg Grating (FBG) sensors appear to be a better choice for surgical robots because of small sizes, high sensitivity, flexibility, biocompatibility, non-toxicity, chemical inertness, immunity to electromagnetic noise and electrical passivity. Compared to other optical fiber sensors, FBG sensors are structurally simple and is not limited by phase discontinuity or intensity fluctuations [24]. Pullteap et. al [25] embedded FBG sensors in a robotic MIS gripper to detect the grasping force and axial force. Iordachita et. al [26] employed FBG sensors for 2 DOF force sensing in retinal surgery. A 3 DOF force sensing pick instrument (ø0.8 mm) was further developed for vitreoretinal surgery, where four FBG sensors were used to maximize the decoupling between axial and transverse force sensing [27]. In the field of shape sensing, Park et. al [28] introduced a biopsy needle integrated with FBGs to detect its bending deflection when inserted in to tissue. Sefati et. al [29] developed a FBG array for real-time large deflection shape sensing of a continuum dexterous manipulator.

For distal end haptic sensing of TSMs, in this paper, we propose to measure the compression force on the sheath at the distal end so that the tension force on the tendon, which equals the compression force on the sheath (theoretically and experimentally confirmed in Section II), can be obtained. This is achieved through a new FBG force sensor which consists of a nitinol tube attached with a FBG strain sensor[1]. The nitinol tube extends from the distal end of the sheath, and the tendon goes through the sheath and the nitinol tube. Pulling the tendon will result in compression from the sheath to the nitinol tube and thus strain on the FBG strain sensor. By recording the wavelength shift due to the strain, the compression force from the sheath, which equals the tension force (magnitude) on the tendon, can be calculated.

There are several advantages with the proposed approach and the new sensor. Firstly, the approach measures the total force applied to the end-effector through the transmission mechanism while sensors directly mounted on the end-effector (such as grasper jaws) involve problems of force decoupling. Secondly, considering that the tendon is much smaller and moves and bends frequently, to avoid damage to the sensor and to avoid decoupling elongation and bending, the new force sensor measures the force on the sheath rather than that on the tendon. Thirdly, the sensor can be well integrated with TSMs and the end-effector because of the similar sizes and configurations of the nitinol tube and the sheath. Fourthly, with this less wiring and passive FBG sensor, no noise from electromagnetic interference and no accessories such as amplifiers are needed at the distal end. Lastly, the fiber for the sensor is flexible, and the fibers with diameters less than 0.1 mm are commercially available.

[1] In this paper, "FBG force sensor" refers to the force sensor (with the nitinol tube) proposed in this paper while "FBG strain sensor" refers to the fiber with a strain sensing segment.

The paper is organized as follows. Section II presents the mechanics of TSMs, including theory and the verification experiment. Section III introduces the working principle of general FBG strain sensors and how the new force sensor works with TSMs and an example end-effector (a surgical grasper). Section IV describes sensor calibrations and tests. Section V presents the experimental results and discussion. Finally, Section VI provides the conclusions and directions for future work.

II. Mechanics of Tendon-sheath Mechanisms

A. Force Analysis of Tendon-sheath Transmission System

Consider an infinitesimal segment of a tendon and sheath bent with a constant curvature, as shown in Fig. 1. T is the tension force in the tendon; C is the compression force in the sheath; N is the normal force from the sheath to the tendon; f is the friction force applied by the sheath to the tendon; N' is the normal force from the tendon to the sheath; f' is the friction force applied by the tendon to the sheath; α is the curve angle of this configuration; μ is the friction coefficient between the tendon and sheath; r is radius of the curve in tendon-sheath configuration.

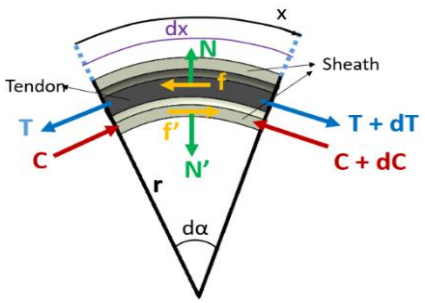

Figure 1. An infinitesimal segment of TSMs in section view (adapted from [30])

For the tendon, applying the force equilibrium equations for a small portion dx, with a corresponding angle dα, the following four equations are obtained [12].

$$Td\alpha = -N,\ d\alpha = dx/r,\ f = \mu N \text{ and } dT = f; \qquad (1\text{-}4)$$

, where the loss of tension force is assumed to be caused only by the friction between the tendon and the sheath [12, 31]. Similar relationships also exist for the sheath:

$$Cd\alpha = -N',\ d\alpha = dx/r,\ f' = \mu N' \text{ and } dC = f'. \qquad (5\text{-}8)$$

Based on Newton's Third Law,

$$N = -N',\ f = -f'. \qquad (9\text{-}10)$$

Thus,

$$Td\alpha = -Cd\alpha. \qquad (11)$$

Then, the crucial fundamental equations for this work are obtained:

$$T = -C;\ dT = -dC \text{ [30]} \qquad (12\text{-}13)$$

Therefore, the magnitude of the compression force on the sheath equals that of the tension force on the tendon at the same cross section. This fact was further experimentally verified, as presented in the following subsection.

Note that both ends of the sheaths are fixed and the configuration keeps still when the endoscopic surgical robot reaches the target operating site. Hence, except the friction forces from the tendons, no other friction force is applied to the sheaths since they do not have the tendency to move.

B. T=-C Verification Experiment

A platform was set up to verify Eq. (12), as shown in Fig. 2. Four hollow compression load cells were utilized to measure the compression force on the sheath and the tension force on the tendon at both the proximal end and the distal end. Since these load cells can only measure compression, the tension on the tendon was converted to compression using a linear slider. A motor was employed to pull the tendon at the proximal end, and a spring was attached to the tendon at the distal end. The flexible configuration of the sheath and tendon was arbitrarily set and fixed by pins on the black foam. Refer to Appendix for the detailed information of the components used.

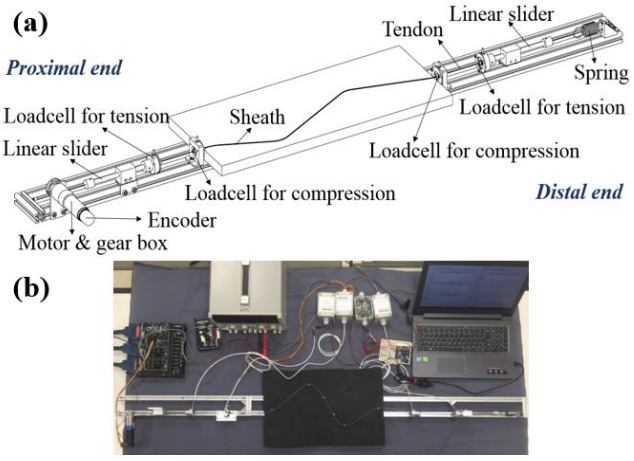

Figure 2. (a) Schematic diagram of experiment setup for T = -C test. (b) Experiment setup for T = -C test.

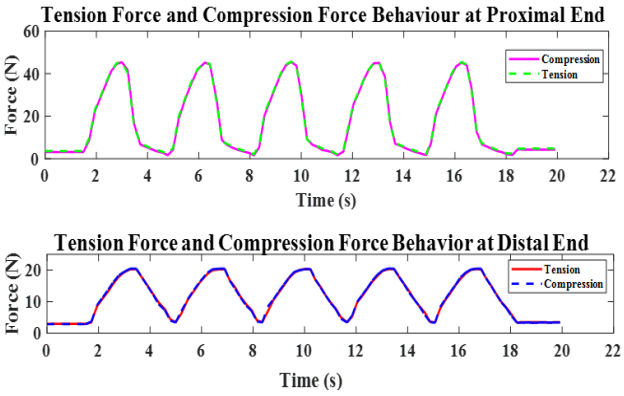

Figure 3. T = -C test result at the proximal end and distal end

A sinewave signal, with an amplitude of 1 and a frequency of 0.3 Hz, was sent to the motor to drive the tendon, and the load cells recorded the associated forces, as shown in Fig. 3. As can be seen, the difference between the tension and compression at the proximal end was 1.75%, and the difference between the tension and compression at the distal end was 0.42%. These errors were mainly because of the noise of the load cells. The experiment result verifies that the compression force of the sheath has almost the same magnitude as the tension force of the tendon at both the distal end and the proximal end. Thus, the relationship of the compression force and the tension force at the distal end, namely T = -C, is valid. Based on this fact, in this paper, we propose to measure the compression on the sheath at the distal end using a FBG force sensor (details are presented below) so that the tension on the tendon at the distal end can be obtained.

III. METHODOLOGY

A. Working Principle of FBG

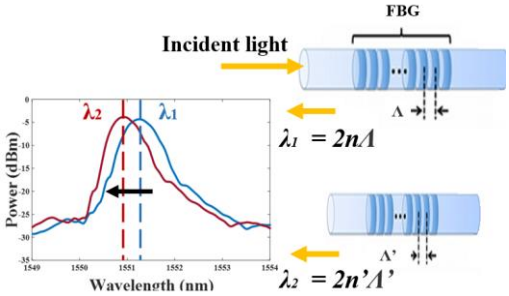

Figure 4. FBG working principle

FBG is a type of distributed Bragg reflector constructed in a short segment of optical fiber. With a periodic variation in the refractive index of the fiber core, FBG is capable of reflecting a particular band of light that shifts in response to variations in temperature and/or strain, as shown in Fig. 4. The central wavelength of the reflection band is called Bragg wavelength λ_B [32]:

$$\lambda_B = 2n_{eff}\Lambda \tag{14}$$

, where n_{eff} represents the effective refractive index of the fiber core mode and Λ is the core refractive index modulation. The parameters n_{eff} and Λ are dependent on temperature and strain. The Bragg wavelength shift with respect to strain and temperature variations is given in Ref. [33]:

$$\frac{\Delta\lambda_B}{\lambda_B} = K_T\Delta T + K_S\Delta\varepsilon \tag{15}$$

, where ΔT , $\Delta\varepsilon$ and $\Delta\lambda_B$ are the change of temperature, axial strain along the fiber, and the caused shift of the central wavelength, respectively. K_T and K_S are the thermal sensing coefficient and strain sensing coefficient of the fiber material. The change of the axial strain along the fiber can cause the central wavelength to shift linearly, which offers an effective way to measuring the loading force by tracking the Bragg wavelength.

B. FBG Force Sensor

For haptic feedback in surgical robots, it is highly desirable to know the force applied to the end-effector by the tendon at the distal end. In this paper, based on Eq. (12), we propose a FBG force sensor to measure the compression force on the sheath at the distal end so that the force applied to the end-effector by the tendon can be obtained.

Fig. 5a depicts the working principle of the force sensor. A nitinol tube is placed at the distal end of the sheath, and the FBG strain sensor is glued to the outer surface of the nitinol tube. The tendon goes through both the sheath and the nitinol tube. When integrated with the end-effector, the “m” end of

the nitinol tube is fixed to the end-effector; pulling the tendon at the proximal end will result in a compression force from the sheath to the nitinol tube. This compression will further result in strain in the FBG strain sensor, and central wavelength will shift in the reflected spectrum of FBG. Based on the wavelength shift, the compression force on the sheath at the distal end can be calculated. Thus, the tension force on the tendon at the distal end can be obtained based on Eq. (12). Fig. 5b shows a prototype of this sensor with a tendon-sheath mechanism.

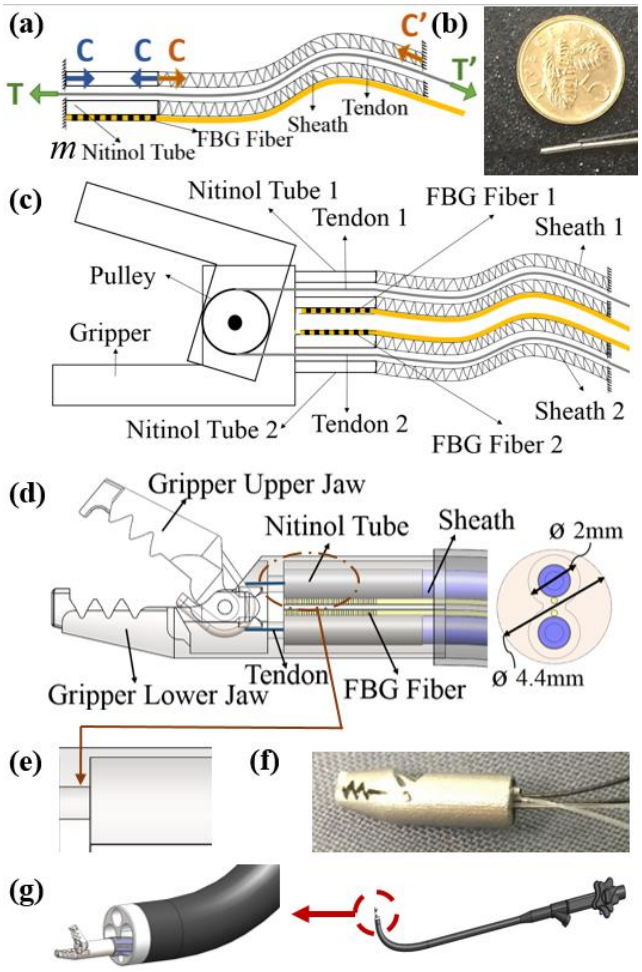

Figure 5. (a) Force analysis between nitinol tube and TSMs. (b) Prototype of FBGs with TSMs. (c) Schematic diagram of the integrated grasper (FBG sensor is shown in dot line). (d) 3D Model of the integrated grasper. (e) Step hole design inside grasper. (f) Prototype of the integrated grasper. (g) Grasper integrated with FBGs insides an endoscope.

Fig. 5c describes how two FBG force sensors are attached to a grasper which consists of two pivotally connected jaws. In this work, two TSMs controls this one degree of freedom. The lower jaw in this example cannot be rotated and thus also severs as the body structure of the grasper. The upper jaw can be bi-directionally rotated by the two tendons fixed to it. Each tendon-sheath has one force sensor. Each tendon extends from the upper jaw to its associated sensor tube and sheath. The sensor can measure the compression force on its associated sheath and thus the tension force on the associated tendon can be obtained. The 3D model and prototype of the grasper integrated with the sensors and tendon-sheath mechanisms are shown in Fig. 5d and 5f. The installation of the FBG-integrated grasper insides an endoscope is presented in Fig. 5g.

As shown in Fig. 5d, a 4 mm long FBG strain sensor (OD: 0.245 mm) is attached on a 6mm tube nitinol (OD: 1.27 mm, ID: 0.97 mm) using super glue, which is then inserted into the step hole (ø 2 mm, shown in Fig. 5e) on the body structure of the grasper. The sheath directly connects with the nitinol tube and a 1 mm long segment of the sheath (OD: 1.189 mm, ID: 0.72 mm) stays inside the step hole to secure good contact with tube. In this study, another 3 mm FBG strain sensor with the same nitinol tube was also developed for exploration.

In this work, nitinol tube was selected because of its super elasticity and biocompatibility. Compared to other biocompatible metal materials such as stainless steel 304/316, with the same dimensions and loads, the strain of the nitinol tube is much larger and thus is more measurable. Moreover, the super elasticity of nitinol provides the sensor with larger strain limit and longer fatigue life. In addition, both the nitinol tube and the sheath are hollow and have similar dimensions; thus, the integration of the sensor with the grasper and the tendon-sheath mechanisms is compact.

IV. SENSOR CALIBRATIONS AND DEMONSTRATION

A. *Sensor Calibrations*

Fig. 6 illustrates the platform with two separate lanes to obtain FBG force sensitivities of the two sensors, respectively. In each lane, a motor pulls the tendon, which passes through a sheath stopper, a sheath, a FBG support and ends at a load cell mounted on a linear slider which is connected with a spring of constant stiffness (0.52N/mm). The sensor, along with a 1 mm long segment of the sheath is inserted into the step hole (as in Fig. 6(c)) of the FBG support. The load cell measures the tension force at the distal end, as a reference to the compression force measured in the sheath/nitinol.

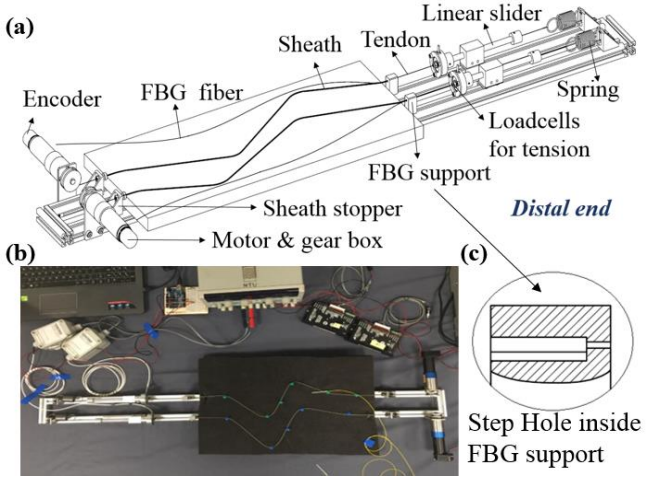

Figure 6. (a) Schematic diagram of platform setup for sensor calibrations. (b) Platform setup for sensor calibrations. (c) Step hole inside FBG support.

Recoating was applied to the grating area in order to protect the FBG strain sensors. Optical spectrum analyzer (Yologawa AQ6370C) was used to track the wavelength of these FBGs.

Tension forces ranging from 0 N to 40N were applied in each lane, and the corresponding wavelength shifts of the

sensors were recorded. With the recorded tension forces and wavelength shifts, the FBG force sensitivity can be obtained. This test was run for three times for 3mm FBG force sensor and four times for 4mm FBG force sensor in order to confirm the repeatability of the sensors.

B. Gasper Demonstration

At the end, a demonstration of a grasper integrated with FBG sensors is present. The demonstration platform is shown in Fig. 7. Basically, instead of lying inside the FBG support, these two FBG force sensors were inserted into the step holes on the body structure of the grasper to measure the tension forces on the two tendons, respectively. The grasper was driven to half open, fully open, and fully closed by the motors through the tendons, as shown in Fig. 8. Refer to Appendix for the detailed information of the components used.

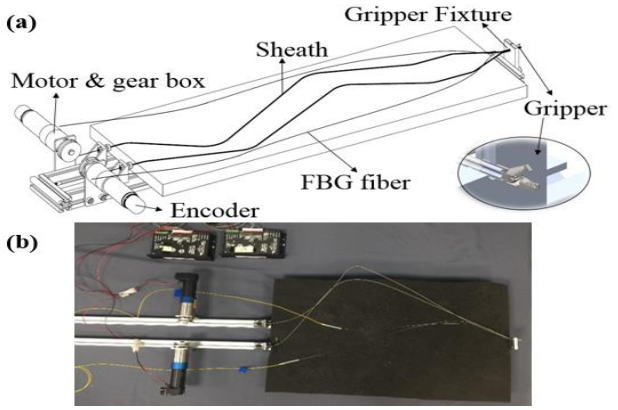

Figure 7. (a) Schematic diagram of platform to demonstrate integrating FBG with grasper. (b) Platform to demonstrate integrating FBG with grasper.

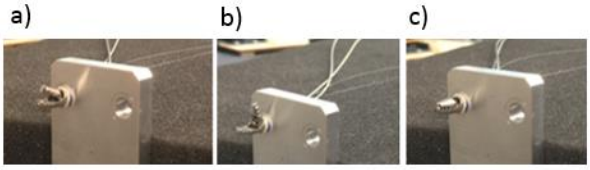

Figure 8. Grasper demonstration: a) Half open, b) fully open and c) fully closed

V. Experiment Results and Discussion

The sensitivity and repeatability test results are presented as follows. Fig. 9a and 9c show the wavelength shifts in response to the forces ranging from 0N to 40N with an increment around 10N. Note that in the tests, the increment was 5N but the results with 10 N increment are shown here only for clarity of figures. The application of this force sensor is suitable for TSM-driven systems, not limited to the flexible surgical robot. Generally the distal end force of robotic surgery is around 0 to 30N. Force up to 40N was tested for exploration purpose. The sidelobes in the spectrum of 4mm FBG in Fig 9a was caused by the optical interference between the adjacent grating fringes in uniform FBG, which cannot be eliminated theoretically due to the nature of the uniform FBG. According to the force sensitivity and repeatability results shown in Fig. 9b and Fig. 9d, two FBG force sensors are capable of detecting forces at the distal end. As shown in Fig. 9b, there is a linear relationship between wavelength shifts and forces for the 4mm FBG, with a force sensitivity of 7.92 pm/N and an adj. R-Square of 0.95. The force sensor with 3 mm grating length has a relatively high force sensitivity of 24.28 pm/N and an adj. R-Square of 0.99, as shown in Fig. 9d. Note that the sensitivity is expressed in pm/N while the slope in Fig. 9b and Fig. 9d is expressed in nm/N. The errors shown in Fig. 9b and Fig. 9d resulted from the signal noise of the load cells and the variant bonding condition between tube and FBGs. The quality of the glue could be the dominant noise source. The sensitivity variance between 3mm and 4mm FBG was also caused by the different bonding condition between the FBG and nitinol tube. In this case, 3mm FBG had a better contact with the tube. Due to the limitations of the current attaching setup for the strain senor and the nitinol tube, there were some uncertainties on the amount of glue applied and the bonding condition between the tube and the strain sensor.

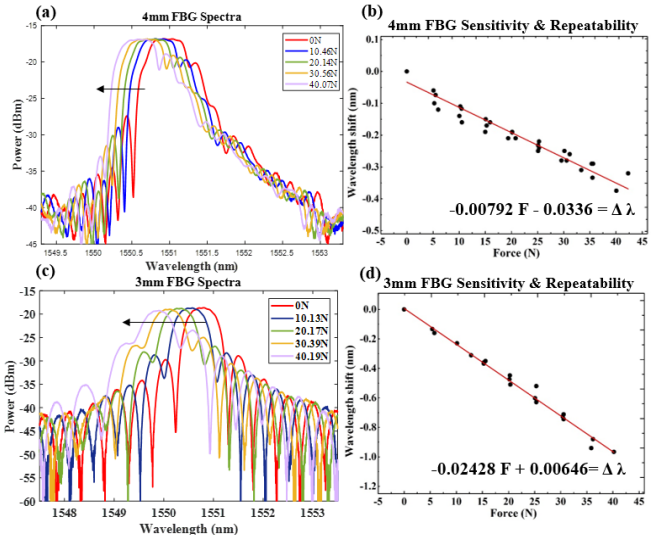

Figure 9. (a) Spectra of 4mm FBG with different loadings. (b) 4mm FBG force sensitivity/repeatability. (c) Spectra of 3mm FBG under different loadings. (d) 3mm FBG force sensitivity/repeatability.

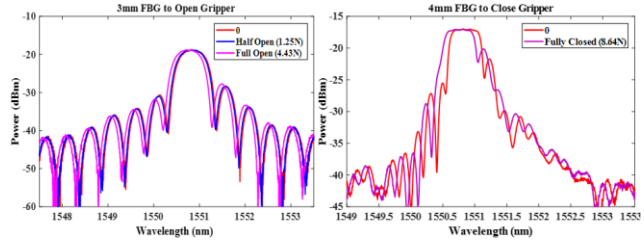

Figure 10. The FBG force readings from grasper demonstration

Relevant wavelength shifts for both FBG sensors are shown in Fig. 10. Corresponding tension forces of the tendons at the distal end were calculated based on the respective wavelength shifts: 1.25N, 4.43N, and 8.64N for the half open, fully open, and fully closed configurations, respectively.

VI. Conclusion

In this paper, we theoretically and experimentally confirmed that the compression force on the sheath and the tension force on the tendon at the same cross-section of a tendon-sheath mechanism are equal in magnitudes. Based on this, a new approach for the haptic sensing in tendon-sheath

driven surgical robots by measuring the distal end compression force on the sheath using a new FBG force sensor was proposed. A FBG strain sensor is attached on a nitinol tube and then integrated with the tendon and sheath on a surgical end-effector. Based on the force sensitivity/repeatability tests, the force sensors can provide the compression force values, which reflect the tension force of tendon at the distal end. The proposed approach and the new FBG force sensor have several salient features, e.g., no need for the decoupling of forces in different directions on the end-effector and the decoupling of elongation and bending on tendons; electrical passivity, compact integration with TSMs, and MRI-compatibility.

Currently, the sensor with 3mm FBG grating length presents the highest sensitivity~24.28 pm/N. The sensor with the nitinol tube is 6 mm long, which is limited by the grating size of the FBG sensor. In the future, force sensors with shorter FBG grating sizes such as 1mm will be explored for end-effectors of multi degrees of freedom. Meanwhile, dual FBGs temperature compensation will be conducted to offset the cross influence of temperature. To improve resolution and accuracy, various types of epoxy will be explored, and optimized nitinol tubular structures will be designed through topology optimization [34,35]. In addition, to secure the contact between nitinol tube and sheath, it is recommended to weld the nitinol tube and sheath as an entire part, which will also further reduce the size of tool connection portion. Furthermore, Micron Optics SM130 or SI255 interrogator will be utilized to automatically trace the real-time central wavelength shifts for FBGs.

The proposed approach and sensor can be applied not only for flexible endoscopic surgical robots, but also for a variety of other TSM-driven systems, such as robotic fingers/hands, wearable devices, and rehabilitation devices.

APPENDIX

TABLE I. COMPONENTS LIST OF SYSTEM

Component	Model	Company	Country
Motor controller	QPIDe	Quanser	Canada
Motor driver	30/1S 134:1	Faulhaber Minimotor SA	Swiss
Motor	2642W024CR 354	Faulhaber Schonaich	Germany
Motor encoder	HEDS-5540 A14	Faulhaber Minimotor SA	Swiss
Motor amplifier	Brush PWM Servo	Advanced Motion Controls	USA
Loadcell controller	Uno	Arduino	Italy
Loadcell	LW1025-25	Interface	USA
Loadcell amplifier	DCA Strain Gage	Interface	USA
Spring	6843	Misumi	Japan
Nitinol tube	NI207130	Goodfellow	England
Sheath	X0620116	Asahi Intecc	Japan
Tendon	Teflon Coated, 0.4mm,	Asahi Intecc	Japan
	Stainless steel		
Fiber	SMF-28	Corning	USA
Optical spectrum analyzer	AQ6370C	Yokogawa	Japan

ACKNOWLEDGMENT

This work was supported by the National Research Foundation (NRF) Singapore (NRFI2016-07).

REFERENCES

[1] S. Frampton and R. L. Kneebone, "John Wickham's New Surgery: 'Minimally Invasive Therapy', Innovation, and Approaches to Medical Practice in Twentieth-century Britain," *Social History of Medicine*, vol. 30, pp. 544-566, 2017.

[2] C. Staub, K. Ono, H. Mayer, A. Knoll, H. Ulbrich, and R. Bauernschmitt, "Remote Minimally Invasive Surgery - Haptic Feedback and Selective Automation in Medical Robotics," *Applied Bionics and Biomechanics*, vol. 8, 2011.

[3] S. J. Phee, A. P. Kencana, V. A. Huynh, Z. L. Sun, S. C. Low, K. Yang, *et al.*, "Design of a master and slave transluminal endoscopic robot for natural orifice transluminal endoscopic surgery," *Proceedings of the Institution of Mechanical Engineers, Part C: Journal of Mechanical Engineering Science*, vol. 224, pp. 1495-1503, 2010.

[4] C. M. Oliveira, H. T. Nguyen, A. R. Ferraz, K. Watters, B. Rosman, and R. Rahbar, "Robotic Surgery in Otolaryngology and Head and Neck Surgery: A Review," *Minimally Invasive Surgery*, vol. p. 11, 2012.

[5] S. Ehrampoosh, M. Dave, M. A. Kia, C. Rablau, and M. H. Zadeh, "Providing haptic feedback in robot-assisted minimally invasive surgery: A direct optical force-sensing solution for haptic rendering of deformable bodies," *Computer Aided Surgery*, vol. 18, pp. 129-141, 2013.

[6] A. M. Okamura, "Haptic Feedback in Robot-Assisted Minimally Invasive Surgery," *Current opinion in urology*, vol. 19, pp. 102-107, 2009.

[7] Y. Kobayashi, P. Moreira, C. Liu, P. Poignet, N. Zemiti, and M. G. Fujie, "Haptic feedback control in medical robots through fractional viscoelastic tissue model," in *2011 Annual International Conference of the IEEE Engineering in Medicine and Biology Society*, pp. 6704-6708, 2011.

[8] R. J. Webster and B. A. Jones, "Design and Kinematic Modeling of Constant Curvature Continuum Robots: A Review," *The International Journal of Robotics Research*, vol. 29, pp. 1661-1683, 2010.

[9] J.-J. Lee and L.-W. Tsai, "The Structural Synthesis of Tendon-Driven Manipulators Having a Pseudotriangular Structure Matrix," *The International Journal of Robotics Research*, vol. 10, pp. 255-262, 1991.

[10] T. N. Do, T. Tjahjowidodo, M. W. S. Lau, and S. J. Phee, "A new approach of friction model for tendon-sheath actuated surgical systems: Nonlinear modelling and parameter identification," *Mechanism and Machine Theory*, vol. 85, pp. 14-24, 2015.

[11] V. Hassani, T. Tjahjowidodo, and T. N. Do, "A survey on hysteresis modeling, identification and control," *Mechanical Systems and Signal Processing*, vol. 49, pp. 209-233, 2014.

[12] M. Kaneko, T. Yamashita, and K. Tanie, "Basic considerations on transmission characteristics for tendon drive robots," in *Advanced Robotics, 1991. 'Robots in Unstructured Environments', 91 ICAR., Fifth International Conference on*, pp. 827-832 vol.1, 1991.

[13] L. Chen and X. Wang, "Modeling of the tendon-sheath actuation system," in *2012 19th International Conference on Mechatronics and Machine Vision in Practice (M2VIP)*, pp. 489-494, 2012.

[14] Z. Wang, Z. Sun, and S. J. Phee, "Haptic feedback and control of a flexible surgical endoscopic robot," *Computer Methods and Programs in Biomedicine*, vol. 112, pp. 260-271, 2013.

[15] J. Rosen, B. Hannaford, M. P. MacFarlane, and M. N. Sinanan, "Force controlled and teleoperated endoscopic grasper for minimally invasive surgery-experimental performance evaluation," *IEEE Transactions on Biomedical Engineering*, vol. 46, pp. 1212-1221, 1999.

[16] G. Tholey, A. Pillarisetti, W. Green, and J. P. Desai, "Design, Development, and Testing of an Automated Laparoscopic Grasper with

3-D Force Measurement Capability," in *Medical Simulation: International Symposium, ISMS 2004, Cambridge, MA, USA, June 17-18, 2004. Proceedings*, S. Cotin and D. Metaxas, Eds., ed Berlin, Heidelberg: Springer Berlin Heidelberg, pp. 38-48, 2004.

[17] K. Tadano and K. Kawashima, "Development of a Master Slave System with Force Sensing Using Pneumatic Servo System for Laparoscopic Surgery," in *Proceedings 2007 IEEE International Conference on Robotics and Automation*, pp. 947-952, 2007.

[18] P. Valdastri, K. Harada, A. Menciassi, L. Beccai, C. Stefanini, M. Fujie, *et al.*, "Integration of a Miniaturised Triaxial Force Sensor in a Minimally Invasive Surgical Tool," *IEEE Transactions on Biomedical Engineering*, vol. 53, pp. 2397-2400, 2006.

[19] R. D. Howe, W. J. Peine, D. A. Kantarinis, and J. S. Son, "Remote palpation technology," *IEEE Engineering in Medicine and Biology Magazine*, vol. 14, pp. 318-323, 1995.

[20] M. V. Ottermo, O. Stavdahl, and T. A. Johansen, "Palpation instrument for augmented minimally invasive surgery," in *2004 IEEE/RSJ International Conference on Intelligent Robots and Systems (IROS) (IEEE Cat. No.04CH37566)*, pp. 3960-3964 vol.4, 2004.

[21] T. Ohtsuka, A. Furuse, T. Kohno, J. Nakajima, K. Yagyu, and S. Omata, "Application of a new tactile sensor to thoracoscopic surgery: experimental and clinical study," *Ann Thorac Surg*, vol. 60, pp. 610-3; discussion 614, 1995.

[22] J. Peirs, J. Clijnen, D. Reynaerts, H. V. Brussel, P. Herijgers, B. Corteville, *et al.*, "A micro optical force sensor for force feedback during minimally invasive robotic surgery," *Sensors and Actuators A: Physical*, vol. 115, pp. 447-455, 2004.

[23] R. K. J, "Applications of MEMS in surgery," *Proceedings of the IEEE*, vol. 92, pp. 43-55, 2004.

[24] A. A. G. Abushagur, N. Arsad, M. Ibne Reaz, A. Ashrif, and A. Bakar, "Advances in Bio-Tactile Sensors for Minimally Invasive Surgery Using the Fibre Bragg Grating Force Sensor Technique:A Survey," *Sensors (Basel, Switzerland)*, vol. 14, pp. 6633-6665, 2014.

[25] S. Pullteap, "Development of an optical fiber-based interferometer for strain measurements in non-destructive application," *Electrical Engineering*, vol. 99, pp. 379-386, 2017.

[26] I. Iordachita, Z. Sun, M. Balicki, J. U. Kang, S. J. Phee, J. Handa, *et al.*, "A sub-millimetric, 0.25 mN resolution fully integrated fiber-optic force-sensing tool for retinal microsurgery," *International Journal of Computer Assisted Radiology and Surgery*, vol. 4, pp. 383-390, 2009.

[27] X. He, J. Handa, P. Gehlbach, R. Taylor, and I. Iordachita, "A Submillimetric 3-DOF Force Sensing Instrument With Integrated Fiber Bragg Grating for Retinal Microsurgery," *IEEE Transactions on Biomedical Engineering*, vol. 61, pp. 522-534, 2014.

[28] Y. L. Park, S. Elayaperumal, B. Daniel, S. C. Ryu, M. Shin, J. Savall, *et al.*, "Real-Time Estimation of 3-D Needle Shape and Deflection for MRI-Guided Interventions," *IEEE/ASME Transactions on Mechatronics*, vol. 15, pp. 906-915, 2010.

[29] S. Sefati, F. Alambeigi, I. Iordachita, M. Armand, R. J. Murphy, and M. Armand, "FBG-based large deflection shape sensing of a continuum manipulator: Manufacturing optimization," in *2016 IEEE SENSORS*, pp. 1-3, 2016.

[30] S. j. Phee, S. c. Low, P. Dario, and A. Menciassi, "Tendon sheath analysis for estimation of distal end force and elongation for sensorless distal end," *Robotica*, vol. 28, pp. 1073-1082, 2010.

[31] G. Palli and C. Melchiorri, "Model and control of tendon-sheath transmission systems," in *Proceedings 2006 IEEE International Conference on Robotics and Automation, 2006. ICRA 2006.*, pp. 988-993, 2006.

[32] K. O. Hill and G. Meltz, "Fiber Bragg grating technology fundamentals and overview," *Journal of Lightwave Technology*, vol. 15, pp. 1263-1276, 1997.

[33] T. Erdogan, "Fiber grating spectra," *Journal of Lightwave Technology*, vol. 15, pp. 1277-1294, 1997.

[34] L. Cao, A. T. Dolovich, A. L. Schwab, J. L. Herder, and W. C. Zhang, “Toward a unified design approach for both compliant mechanisms and rigid-body mechanisms: Module optimization,” *Journal of Mechanical Design*, vol. 137, no. 12, p. 122301, 2015.

[35] L. Cao, A. T. Dolovich, and W. C. Zhang, “On understanding of design problem formulation for compliant mechanisms through topology optimization”, *Mechanical Sciences*, vol. 4, no. 2, pp.357-369, 2013.